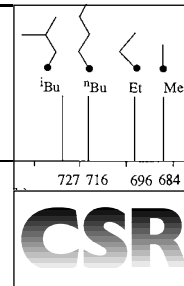


# Probing organometallic structure and reactivity by transition metal NMR spectroscopy†



Wolfgang von Philipsborn

Organisch-chemisches Institut, Universität Zürich, Winterthurerstrasse 190, CH-8057 Zürich, Switzerland

Received (in Cambridge) 4th August 1998

Transition metal NMR chemical shifts are readily measured by modern 1D and 2D pulse techniques and serve as a probe into electronic and steric effects of ligands and substituents in metal complexes. Quantitative correlations of metal chemical shifts with reaction rates and catalytic activities, both experimental and as a result of quantum chemical calculations, give new mechanistic insights and permit reactivity predictions and a screening of homogeneous catalysts. A variety of such examples involving the spin-1/2 nuclei  $^{57}\text{Fe}$ ,  $^{103}\text{Rh}$ , and  $^{187}\text{Os}$  as well as the quadrupolar nuclei  $^{51}\text{V}$ ,  $^{53}\text{Cr}$ ,  $^{55}\text{Mn}$ ,  $^{59}\text{Co}$ , and  $^{91}\text{Zr}$  are discussed.

## 1 Introduction

The concept of reactivity, both in the qualitative and quantitative sense, is of prime importance in chemistry. Therefore, chemists have always explored methods to predict the reactivity of molecules, and for this the use of physical probes and theoretical models has proved useful and generally applicable. In organometallic chemistry the problem is particularly complex and demanding because of the chemical variety of the

metals and their manifold coordination and binding properties. An even greater challenge constitutes the prediction of catalytic activity in homogeneous systems, a problem of topical interest in current chemical research.

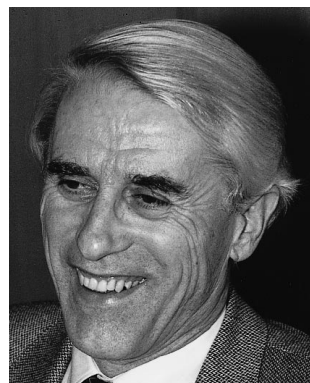
Nuclear magnetic resonance (NMR) spectroscopy appears to offer a particularly suitable and promising probe into chemical reactivity as it is element-specific and applicable to any metal of the periodic system providing an isotope with a nuclear spin.<sup>2–4</sup> Transition metal NMR has the advantage over the more commonly known proton NMR for several reasons. Firstly, hydrogen is a peripheral atom in most organometallic structures, except hydrides, whereas the reactivity is associated with the coordination centre. Secondly, transition metal nuclei offer very large shielding (chemical shift) ranges and, hence, higher sensitivity to subtle structural perturbations. On the other hand, they possess small magnetic moments, electric nuclear quadrupole moments if the spin quantum number  $I \geq 1$ , a wide range of (field-dependent) relaxation times for  $I = 1/2$ , very short relaxation times for  $I \geq 1$  and, in general, smaller sensitivities to detection than is known for protons. However, in recent years transition metal NMR has been boosted by dramatic instrumental improvements that have allowed its development from a promising basic research field to a useful and versatile tool in the hands of the organometallic and coordination chemist.<sup>5,6</sup> This has been made possible by a combination of improved instrumentation, high-sensitivity detection methods, and a better data base for an understanding of the structural factors that determine the NMR spectral parameters of the heavier elements, in particular the transition metals. In this progress report, emphasis will lie on the use of transition metal NMR data to rationalize and predict organometallic reactivity and catalytic activity.

## 2 NMR properties of transition metals

The magnetic properties of the transition metal nuclei that are relevant for this review are summarized in Table 1. The corresponding data for other transition metals may be found in ref. 7. Fundamentally different properties are observed for metals with spin-1/2 isotopes and quadrupolar nuclei ( $I \geq 1$ ) since the former exhibit sharp resonance lines whereas the latter may give rise to very broad lines depending on the size of the electric quadrupole moment  $Q$ , and the electric field gradient  $q_{zz}$  that is determined by the symmetry of the electron distribution.<sup>7</sup> For ease of detection in NMR experiments, the size of the magnetic moment  $\mu$  or the magnetogyric ratio  $\gamma = \mu/\hbar$  and the natural abundance of the isotope are of additional importance. Hence, the transition metal nuclei fall into four distinct classes that require different experimental techniques for optimal detection of their resonances, as illustrated in Table 2. Since pulsed excitation depends on the longitudinal ( $T_1$ ) and trans-

† Transition metal NMR spectroscopy. Part 40. For Part 39, see ref. 1.

Wolfgang von Philipsborn was born in 1929 in Germany and studied Chemistry at the Free University in Berlin and the University of Zürich where he received his PhD in 1956. He was appointed Research Associate at the Massachusetts Institute of Technology (1959–60), returned to the University of Zürich in 1961 and established one of the first NMR research groups in Switzerland. He was appointed Lecturer in 1963 and Assistant Professor in 1966. In 1972 he was Visiting Professor at the Israel Institute of Technology in Haifa and from 1974–97 Full Professor at the University of Zürich, where he presently holds an Honorary Professorship.



His current research interests are focused on structural and mechanistic organometallic chemistry and comprise all aspects of high-resolution multi-nuclear NMR, in particular of transition metals. He was awarded the Alfred-Werner Prize (1965), the Centennial Medal of the Case Institute of Technology (Cleveland, 1980), and Honorary Membership of the Swiss Chemical Society (1996).

**Table 1** Magnetic properties of some transition metal nuclei

	<sup>53</sup> Cr	<sup>55</sup> Mn	<sup>57</sup> Fe	<sup>59</sup> Co	<sup>91</sup> Zr	<sup>103</sup> Rh	<sup>183</sup> W	<sup>187</sup> Os
Frequency/MHz (at 14.1 T)	33.8	149.0	19.4	142.2	56.0	18.9	25.3	13.8
% Isotope	9.6	100	2.2	100	11.2	100	14.3	1.6
Spin/ ( $h/2\pi$ )	3/2	5/2	1/2	7/2	5/2	1/2	1/2	1/2
Quadrupole moment / $10^{-28}$ m <sup>2</sup>	0.04	0.40	—	0.42	-0.21	—	—	—
Receptivity( <sup>13</sup> C=1.0)	0.485	1014	0.004	1590	6.0	0.18	0.06	0.001
Chemical shift range/KHz(ppm)	85(2500)	520(3500)	350(18000)	2800(20000)	85(1500)	227(12000)	165(6500)	90(6500)

**Table 2** Detection methods for the four types of transition metal nuclei

<b>I</b>	$I = 1/2$ Large $\gamma$ Short $T_1$	<sup>113</sup> Cd <sup>195</sup> Pt <sup>199</sup> Hg	Normal pulse techniques
<b>II</b>	$I = 1/2$ Small $\gamma$ Long $T_1$	<sup>57</sup> Fe <sup>103</sup> Rh <sup>109</sup> Ag <sup>183</sup> W <sup>187</sup> Os	Normal pulse techniques at high $B_0$ fields, or polarisation transfer from <sup>1</sup> H or <sup>31</sup> P, <i>i.e.</i> INEPT (1D) or HMQC (2D INVERSE)
<b>III</b>	$I \geq 1$ Small $Q$ Short $T_2$	<sup>51</sup> V <sup>53</sup> Cr <sup>91</sup> Zr <sup>95</sup> Mo <sup>99</sup> Ru	Normal pulse techniques
<b>IV</b>	$I \geq 1$ Large $Q$ Very short $T_2$	<sup>55</sup> Mn <sup>59</sup> Co <sup>61</sup> Ni <sup>101</sup> Ru <sup>105</sup> Pd	Normal pulse techniques, preferably at high $B_0$ fields when receptivity is low

verse ( $T_2$ ) relaxation times, which can vary over several orders of magnitude, this information is also included in Table 2 as a guideline.

Whenever possible the NMR experimentalist will choose a spin-1/2 isotope to which powerful sensitivity enhancement techniques can be applied, *e.g.* polarisation transfer from the high- $\gamma$  nuclei <sup>1</sup>H or <sup>31</sup>P that are commonly found in organometallic structures and often spin-coupled to the metal nucleus (Fig. 1). The experiments can be performed in 1D or 2D modes.

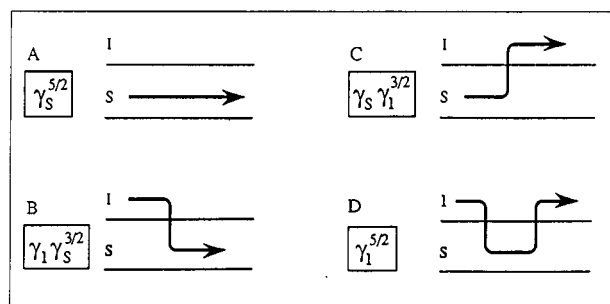


**Fig. 1** Direct (A, B) and indirect (C, D) S-spin detection in an I,S spin system ( $I = ^1\text{H}, ^{19}\text{F}, ^{31}\text{P}$ ;  $S =$  spin-1/2 metal nucleus, *e.g.* <sup>57</sup>Fe, <sup>103</sup>Rh, <sup>187</sup>Os). Sensitivities are proportional to the  $\gamma$ -factors given in the rectangles. The polarisation transfer yields sensitivity enhancement factors, relative to A, of  $(\gamma_I/\gamma_S)$  for B (INEPT),  $(\gamma_I/\gamma_S)^{3/2}$  for C (inverse INEPT), and  $(\gamma_I/\gamma_S)^{5/2}$  for D (INVERSE). For actual values, see Table 3.

Sensitivity enhancement factors obtainable from such pulse techniques are dramatic and permit routine NMR measurements

**Table 3** Intensity gain in <sup>1</sup>H,X NOE and polarisation transfer experiments<sup>a,b</sup>

X =	<sup>13</sup> C	<sup>15</sup> N	<sup>57</sup> Fe	<sup>103</sup> Rh	<sup>183</sup> W	<sup>187</sup> Os
NOE	2.99	-3.93	16.4	-16.8	12.9	22.6
INEPT	3.98	9.86	30.8	31.6	23.7	43.2
Inverse INEPT	7.93	31.0	171	178	115	284
INVERSE (2D)	31.5	305	5263	5610	2737	12 264

<sup>a</sup> Values calculated from magnetogyric ratios  $\gamma$  reported in ref. 7. <sup>b</sup> For <sup>31</sup>P,X experiments, the PT factors are, respectively, 2.47, 3.88, and 9.57 times smaller.

of otherwise 'difficult' nuclei on multinuclear, multichannel NMR instruments, provided that a spin coupling to the metal exists. Table 3 summarizes the calculated enhancement factors *vis-à-vis* normal detection or NOE-enhancement factors. The latter are generally irrelevant for transition metal nuclei as dipolar relaxation is usually unimportant.

The <sup>57</sup>Fe, <sup>103</sup>Rh, and <sup>187</sup>Os NMR spectra that are discussed further below were obtained on three-channel 600 MHz and 400 MHz spectrometers equipped with triple-resonance inverse probeheads optimized for the required low-frequency range and with optional <sup>1</sup>H or <sup>31</sup>P polarisation and decoupling facilities, respectively. The pulse scheme (Fig. 2) is based on the classic

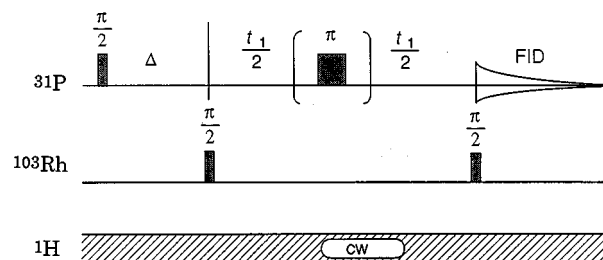


**Fig. 2** Standard HMQC pulse sequence for inverse detection of <sup>103</sup>Rh via <sup>31</sup>P with concomitant <sup>1</sup>H decoupling. The <sup>31</sup>P and <sup>1</sup>H channels can be exchanged. The 180° pulse is optional and removes I,S spin coupling in the  $F_1$  dimension.

HMQC sequence<sup>8,9</sup> and the  $\pi$ -pulse in the  $t_1$  period is applied only when no metal-proton or metal-phosphorus spin coupling is desired on the  $F_1$  axis of the 2D correlation spectrum. Decoupling from the phosphorus (or hydrogen) nuclei in the third channel is optional and may serve as an additional sensitivity enhancing factor for the transition metal signal.<sup>10</sup> An example of the wealth of information that may be obtained from such a single experiment is shown in Fig. 3. It allows us to determine two chemical shifts ( $\delta(\text{H})$ ,  $\delta(\text{Ag})$ ), and five heteronuclear coupling constants ( $^1J(\text{Ag,P})$ ,  $^1J(\text{Ag,H})$ ,  $^1J(\text{Rh,H})$ ,  $^2J(\text{Ag,Rh})$ , and  $^2J(\text{P,H})$ ) in a dinuclear bridged hydride complex.<sup>11</sup> The interesting result here is the rather large two-bond spin interaction of 19 Hz between the low- $\gamma$  Ag and Rh nuclei which may be the consequence of high internuclear electron density from the three bridging hydride ligands. An excellent survey of the various methods for the detection of transition metals using polarisation transfer and indirect or inverse detection was given by D. Nanz.<sup>11</sup>

The detection of quadrupolar transition metal nuclei is usually handicapped by very short transverse relaxation times  $T_2$  requiring rapid acquisition of the FID and resulting in broad

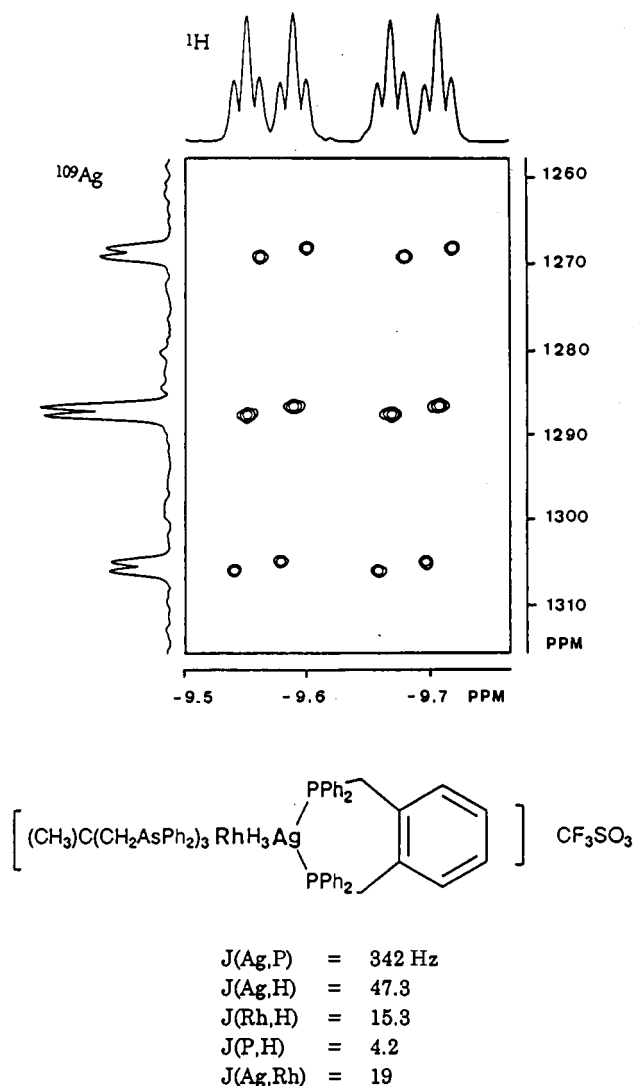


**Fig. 3** ( $^1\text{H}$ ,  $^{109}\text{Ag}$ ) shift-correlation spectrum (HMQC) of a heterodinuclear bridged hydride complex ( $\text{CD}_2\text{Cl}_2$ , 253 K). The  $^{109}\text{Ag}$ ,  $^{103}\text{Rh}$  coupling (19 Hz) is resolved on the  $^{109}\text{Ag}$  axis.<sup>11</sup>

resonance lines devoid of nuclear spin coupling information. In addition, the signal intensity may become so weak that certain transition metal nuclei are extremely difficult to observe, *e.g.*  $^{61}\text{Ni}$  and  $^{105}\text{Pd}$ . Nuclei with high receptivities such as  $^{55}\text{Mn}$ ,  $^{59}\text{Co}$ , and  $^{91}\text{Zr}$  are useful probes for the organometallic chemist, and several examples are presented in this review. In all cases, the resonance lines were obtained by direct detection at high field strengths ( $B_0 = 14.1$  or  $9.4$  T). The practical upper limit for detection of broad lines of quadrupolar nuclei on a commercial high-resolution NMR spectrometer is a line width of about  $\Delta\nu(1/2) = 25\text{--}30$  kHz. Excessive broadening can often be reduced by an application of a non-viscous solvent and elevated temperature, both reducing the molecular rotational correlation time  $\tau_c$  and thereby the relaxation rate  $T_2^{-1}$ .

### 3 Transition metal shielding (chemical shift)

For our purpose of establishing correlations of metal chemical shifts with subtle structural changes and, eventually, differences in chemical reactivity of organometallic complexes, two features of metal shielding are of particular relevance: a) The transition metal nuclei, like those of other heavy elements, exhibit very large chemical shift ranges that may extend to more than ten thousand parts per million (ppm), and thus this parameter becomes extremely sensitive to small changes in the ligand field, *i.e.* the electronic and stereochemical environment.

b) Changes in chemical shift for a given transition metal are largely determined by the *paramagnetic* shielding term  $\sigma_{\text{para}}$  that, unlike the *diamagnetic* term  $\sigma_{\text{dia}}$ , not only depends on electron density at the nucleus but is also related to an electronic excitation energy  $\Delta E^{-1}$ , non-s-orbital expansion terms  $\langle r^{-3} \rangle$ , and p- and d-orbital population terms  $P_u$  and  $D_u$ , respectively (eqn. (1)).<sup>12</sup>

$$\sigma_{\text{para}} \propto -\frac{1}{\Delta E} \times (\langle r^{-3} \rangle_{\text{np}} P_u + \langle r^{-3} \rangle_{\text{nd}} D_u) \quad (1)$$

The term  $\sigma_{\text{para}}$  has the opposite sign to  $\sigma_{\text{dia}}$  that is determined by the inner-core electrons. As a result of eqn. (1) a complex situation arises in which the transition metal chemical shift is influenced by terms related to the nephelauxetic effect of ligands ( $r^{-3}$ ), the energy of electronic d,d-transition energies (*e.g.* charge transfer bands), and changes in binding of coordinated ligands. The individual contributions of the three major sources, however, are difficult to separate. Hence, correlations of metal shielding with these three parameters as well as quantum chemical (*ab initio*) calculations are useful to clarify the interpretation of chemical shift changes in an individual case. For example, the linear relationship between  $^{59}\text{Co}$  chemical shifts in octahedral  $\text{Co}(\text{III})$  complexes  $\text{CoX}_6$  and inverse d,d-transition energies  $\Delta E^{-1}$  has been known since 1957<sup>7</sup> and was confirmed in several other cases. Other correlations with metal–ligand bond lengths from X-ray diffraction<sup>13</sup> and with thermodynamic complex stabilities<sup>14</sup> were published. From a theoretical point of view, however, quantitative correlations of transition metal chemical shifts with rate constants of ligand exchange reactions are particularly interesting; several examples have become known only recently.

During the past few years improved methods for *ab initio* and density functional calculations of multi-electron molecular systems have stimulated theoretical chemists to calculate shielding constants of transition metal nuclei in organometallic and coordination compounds. These *ab initio* calculations may also involve transition states and, hence, give access to energy barriers and thus, in principle, to (relative) reaction rates. Here, the relation to empirical shielding–reactivity correlations becomes particularly challenging, and several recent examples will be discussed further below.

For the heavier transition metals, relativistic effects have been shown to become important. The relativistic contraction of inner shell s and p electron orbitals has large effects on diamagnetic shielding and indirectly affects (expands) d and f electrons which, in turn, is reflected in  $\sigma_{\text{para}}$ . In general, such relativistic effects are expected to be larger for *absolute* shielding values than for the *relative* chemical shift data that are associated with  $\sigma_{\text{para}}$ .<sup>7</sup>

### 4 Correlation with structure and reactivity

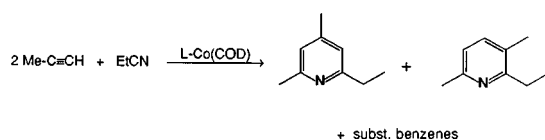
Although the commonly used terms electronic and steric substituent effects are often difficult to separate, changes in chemical reactivity are normally discussed using this terminology. Therefore, we shall briefly discuss the influence of ligand structure on transition metal shifts.

Early examples from  $^{57}\text{Fe}$ ,  $^{59}\text{Co}$ , and  $^{103}\text{Rh}$  NMR have clearly shown that shielding of the metal nucleus in  $\eta^4(\text{diene})$  complexes *decreases* with the electron-attracting power of substituents on the diene system and with increasing steric requirements of alkyl substituents.<sup>3,15,16</sup> These findings were confirmed in the two series of octahedral alkylcobaloximes<sup>13</sup> and alkylrhodoximes<sup>17</sup> where quantitative correlations of  $\delta(^{59}\text{Co})$  and  $\delta(^{103}\text{Rh})$  with both electronic and steric substituent parameters were established. The steric deshielding effects also correlate with the metal–carbon bond length and calculated bond dissociation energies and thus can be traced back to a

weakening of the bond. Further examples involving quantitative correlations of metal shielding with steric substituent parameters  $\theta$  (Tolman) and  $E_s$  (Taft) will be discussed towards the end of this section.

A considerable amount of work has been invested recently in determining the spatial arrangement and dynamics of ligands in organometallic complexes in solution using state-of-the-art 2D NMR techniques, *i.e.* NOESY, ROESY, and EXSY. Most of these studies have been carried out with the aid of  $^1\text{H}$ ,  $^{13}\text{C}$  or  $^{31}\text{P}$  NMR and, therefore, they will not be discussed in this review. For leading references see ref. 18.

We will now focus on a novel application to mechanistic organometallic chemistry, *i.e.* probing the reactivity of transition metal complexes in stoichiometric and catalytic reactions by transition metal chemical shifts. In the first published example that stimulated our further studies, the cobalt-catalyzed cyclization of alkynes and nitriles to form substituted pyridines,  $\delta^{59}\text{Co}$  of (R-Cp)Co(COD) and (R-indenyl)Co(COD) complexes was found to correlate with their catalytic activity expressed as the temperature  $T$  at which 65% of the propyne is transformed continuously to products (Bönnemann<sup>19</sup>) (Scheme 1). In both catalytic series  $^{59}\text{Co}$  shielding decreases



with increasing reactivity of the catalyst and increasing electron acceptor property of R (Fig. 4). Eqns. (2) (for RCpCo(COD)

$$T/^{\circ}\text{C} = 160.6 - 0.25 \times \delta_{\text{rel}}(^{59}\text{Co}) R = 0.91 \quad (2)$$

catalysts) and (3) (for (R-indenyl)Co(COD) catalysts) were

$$T/^{\circ}\text{C} = 131.6 - 0.17 \times \delta_{\text{rel}}(^{59}\text{Co}) R = 0.98 \quad (3)$$

derived from linear regression analysis. The empirical correlation turned out to be useful in screening a large number of

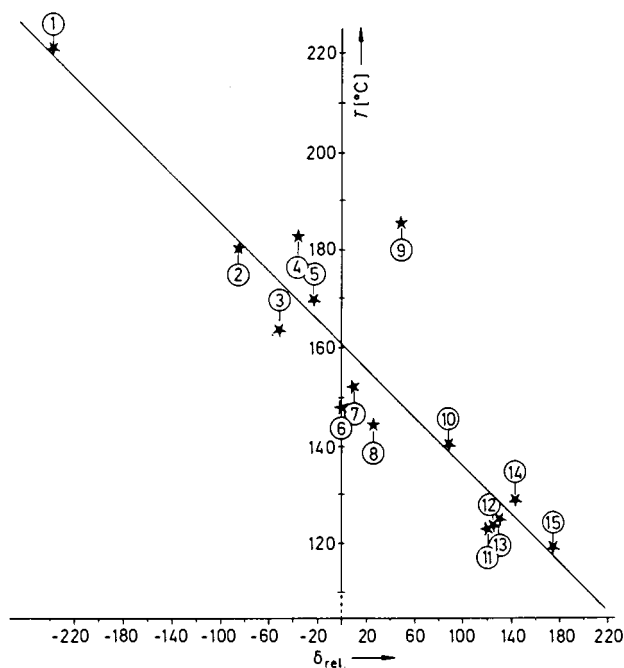
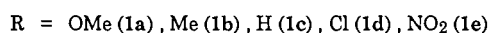
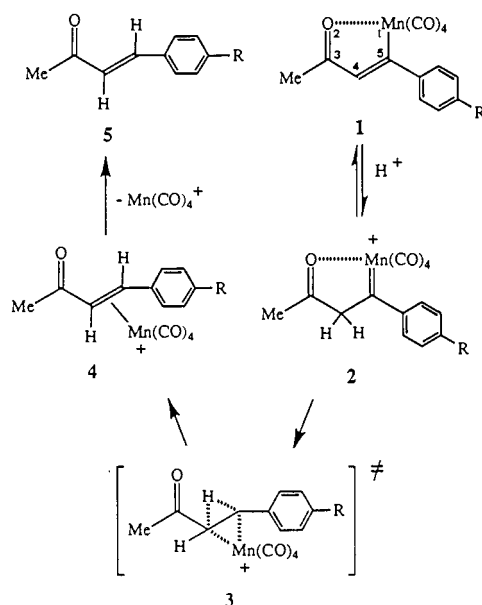


**Fig. 4** Catalytic activity of [YCo(COD)] complexes in the pyridine synthesis (Scheme 1) as a function of the relative  $^{59}\text{Co}$  chemical shifts. Y = substituted cyclopentadienyl ligand; Me<sub>5</sub>C (1), bicyclo[3.3.0]octadienyl (2), MeC<sub>5</sub>H<sub>4</sub> (3), CH<sub>3</sub>CH(OH)C<sub>5</sub>H<sub>4</sub> (4), ClC<sub>5</sub>H<sub>4</sub> (5), C<sub>5</sub>H<sub>5</sub> (6), <sup>t</sup>BuC<sub>5</sub>H<sub>4</sub> (7), Me<sub>3</sub>SiC<sub>5</sub>H<sub>4</sub> (8), CH<sub>2</sub>=C(Me)C<sub>5</sub>H<sub>4</sub> (9), PhC<sub>5</sub>H<sub>4</sub> (10), AcC<sub>5</sub>H<sub>4</sub> (11), C<sub>2</sub>H<sub>5</sub>COC<sub>5</sub>H<sub>4</sub> (12), CH<sub>3</sub>OCOC<sub>5</sub>H<sub>4</sub> (13), OHCC<sub>6</sub>H<sub>4</sub> (14), PhCOC<sub>6</sub>H<sub>4</sub> (15). Reproduced with permission from H. Bönnemann, *Angew. Chem., Int. Ed. Engl.*, 1985, **24**, 248. Copyright (1985) Wiley-VCH.

potential catalysts by simply determining their  $^{59}\text{Co}$  chemical shifts.<sup>20</sup> The catalytic cycle for this reaction<sup>19</sup> involves several ligand substitutions at cobalt, but the activity determining ligands (RCp) and (R-indenyl) remain attached to the metal throughout the sequence of reactions in which the replacement of the two COD ethylenic bonds by alkyne ligands appears to be the rate-determining step. Here the donor/acceptor property of R determines its key function on the reaction rate. The  $^{59}\text{Co}$  shieldings in the 'pre-catalysts' thus seem to model those of the reactive species which cannot be detected by  $^{59}\text{Co}$  NMR. Another early attempt to correlate catalytic strength of metal complexes with transition metal shielding was made in the case of octahedral Ru(II) complexes of the type [RuL<sub>3</sub>]<sup>2+</sup>, [RuL<sub>2</sub>X]<sup>2+</sup>, [RuLX<sub>2</sub>]<sup>2+</sup>, and [RuX<sub>3</sub>]<sup>2+</sup> (L, X = nitrogen donor ligands) which are photosensitizers in the photoreduction of water. It was found that the  $^{99}\text{Ru}$  chemical shift correlates qualitatively with the Ru(II)/Ru(III) oxidation potential that determines the catalytic efficiency of the complex.<sup>21</sup>

Substituent effects on reaction rates and chemical shifts of  $^{55}\text{Mn}$ , another quadrupolar nucleus that can be readily detected, have also been correlated in a demetalation reaction (DeShong) (Scheme 2). In previous studies it was demonstrated that (1) the



Scheme 2

manganacycle underwent reversible protonation at C(4) under acidic conditions, (2) the rate of demetalation was unimolecular in manganacycle **1**, and (3) the rate had a Hammett  $\sigma^+$ -correlation with the *para*-substituent of the aromatic ring ( $\rho = -0.76$ ). The observed linear correlation of  $\log k_{\text{obs}}$  with  $\delta(^{55}\text{Mn})$  of **1a-e** ( $R = 0.956$ , Fig. 5) was remarkable and was the first example of a quantitative relationship between a kinetic parameter and a transition metal chemical shift.<sup>22</sup> We shall discuss the mechanistic implications further below.

Subsequently several other quantitative correlations of this type were discovered in our group for  $^{103}\text{Rh}$  and  $^{57}\text{Fe}$  chemical shifts with the rates of CO-PPh<sub>3</sub> ligand exchange in (X)CpRh(CO)<sub>2</sub> complexes,<sup>23</sup> PPh<sub>3</sub> induced CO insertion in CpFe(CO)<sub>2</sub>R complexes,<sup>5</sup> and PPh<sub>3</sub> induced aryl migration in Cp(Me<sub>5</sub>)Rh(I)(CO)(aryl) complexes.<sup>24</sup> In the first of these examples, the ligand exchange proceeds *via* an associative  $\eta^3$ -allyl-coordinated intermediate (Scheme 3). The correlation of  $\delta(^{103}\text{Rh})$  of the starting complexes with the  $\log k$  values determined by Basolo and Cheong<sup>25</sup> is illustrated in Fig. 6. The strong influence of the substituent X is reflected in the large range of the observed rate constants ( $\sim 4$  orders of magnitude)

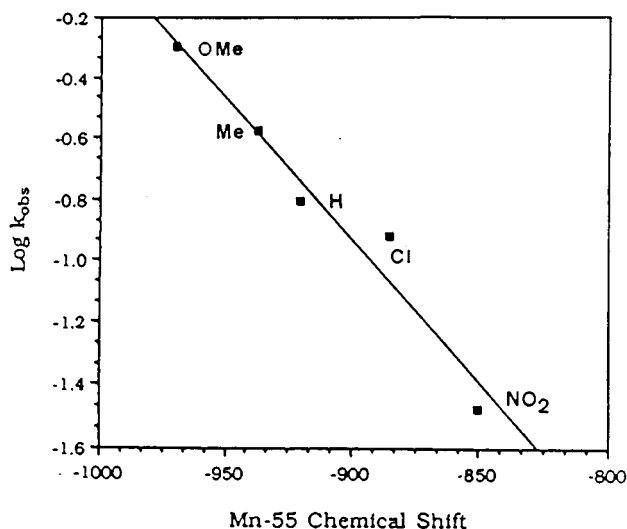
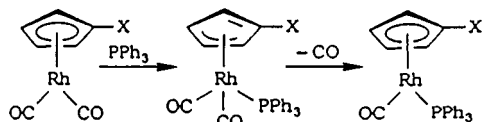


**Fig. 5** Plot of  $\log k_{\text{obs}}$  vs.  $^{55}\text{Mn}$  chemical shifts of the reactant complexes **1a–1e** for the demetalation reaction of manganacycles (Scheme 2),  $R = 0.956$ ; reproduced with permission from P. DeShong, D. R. Sidler, P. J. Rybczynski, A. A. Ogilvie and W. von Philipsborn, *J. Org. Chem.*, 1989, **54**, 5432. Copyright (1989) American Chemical Society.



**Scheme 3** Reproduced with permission from M. Koller and W. von Philipsborn, *Organometallics*, 1992, **11**, 467. Copyright (1992) American Chemical Society.

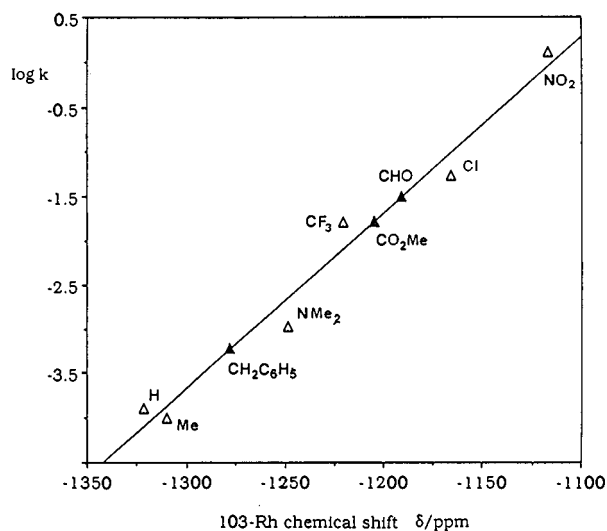
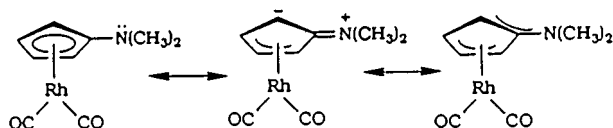


**Fig. 6** Correlation of  $^{103}\text{Rh}$  chemical shifts of substituted (X) $\text{CpRh}(\text{CO})_2$  complexes with rate constants of the carbonyl displacement reaction with  $\text{PPh}_3$  (Scheme 3): ( $\Delta$ ) correlation points; ( $\blacktriangle$ )  $^{103}\text{Rh}$  shifts of complexes for which rates are unknown;  $R^2 = 0.973$ ; reproduced with permission from M. Koller and W. von Philipsborn, *Organometallics*, 1992, **11**, 467. Copyright (1992) American Chemical Society.

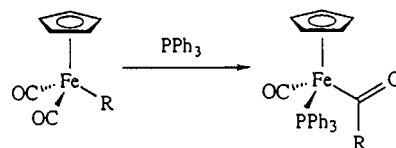
and the chemical shift range of the  $^{103}\text{Rh}$  nucleus ( $\sim 200$  ppm). In contrast with the Hammett plot ( $\log k$  vs.  $\sigma_p$ ) reported by Basolo, the  $(\text{CH}_3)_2\text{N}$ - and Cl-substituted complexes fit into our linear correlation indicating that the  $\pi$ -donor properties of  $\text{N}(\text{CH}_3)_2$  and Cl substituents, responsible for the increased rate of  $\text{PPh}_3$  addition, must also be reflected in the  $^{103}\text{Rh}$  chemical shifts. The decreased shielding can indeed be understood on the

basis of reduced coordination of the metal in the starting complex (Scheme 4).



**Scheme 4** Reproduced with permission from M. Koller and W. von Philipsborn, *Organometallics*, 1992, **11**, 467. Copyright (1992) American Chemical Society.

Whereas the substituent effects in the previous example were largely of an electronic nature, the  $\text{PPh}_3$  induced CO insertion into an Fe–C  $\sigma$ -bond appears to be governed by the steric size of the alkyl ligand  $\text{R}^5$  (Scheme 5). Fig. 7 gives a graphical



**Scheme 5** Reproduced with permission from E. J. M. Meier, W. Kozminski, A. Linden, P. Lustenberger and W. von Philipsborn, *Organometallics*, 1996, **15**, 2469. Copyright (1996) American Chemical Society.

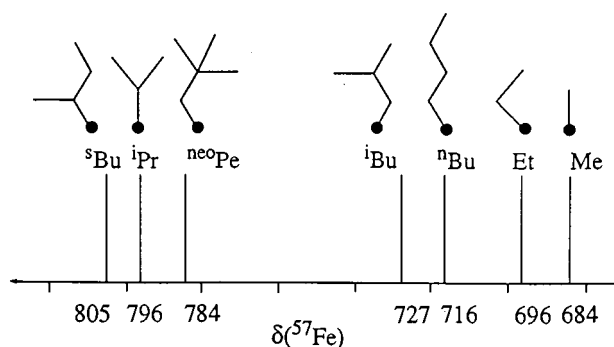
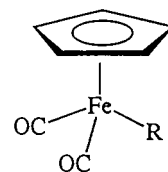


**Fig. 7** Graphical representation of  $^{57}\text{Fe}$  chemical shifts in  $\text{CpFe}(\text{CO})_2\text{R}$  complexes illustrating the steric deshielding effect; reproduced with permission from E. J. M. Meier, W. Kozminski, A. Linden, P. Lustenberger and W. von Philipsborn, *Organometallics*, 1996, **15**, 2469. Copyright (1996) American Chemical Society.

representation of the deshielding of the  $^{57}\text{Fe}$  nucleus induced by the steric inhibition of coordination, and Fig. 8 illustrates the correlation between  $k_{\text{obs}}$  and  $\delta(^{57}\text{Fe})$ . High  $^{57}\text{Fe}$  shielding (*i.e.*, a low-frequency resonance) corresponds to a slow CO insertion reaction and, therefore, a strong Fe–C bond (large  $\Delta H^\ddagger$ ). As no X-ray crystallographic data are available for complexes of this type, density functional calculations of the geometry and bond dissociation energy were carried out for complexes with  $\text{R} = \text{Me}$ , n-Bu, and  $^i\text{Pr}$ . They confirmed our expectations and showed that the metal–alkyl  $\sigma$ -bond distance *increases* and the bond dissociation energy (BDE) *decreases* with the steric demand of R:  $r(\text{Fe}–\text{Me}) = 206.2$  pm;  $\text{BDE} = 217.1$  kJ mol $^{-1}$ ;  $r(\text{Fe}–^n\text{Bu}) = 208.1$  pm;  $\text{BDE} = 196.2$  kJ mol $^{-1}$ ;  $r(\text{Fe}–^i\text{Pr}) = 211.6$  pm;  $\text{BDE} = 170.7$  kJ mol $^{-1}$  (ref. 5; see also Section 5). The changes of  $\delta(^{57}\text{Fe})$  can be explained by referring to the

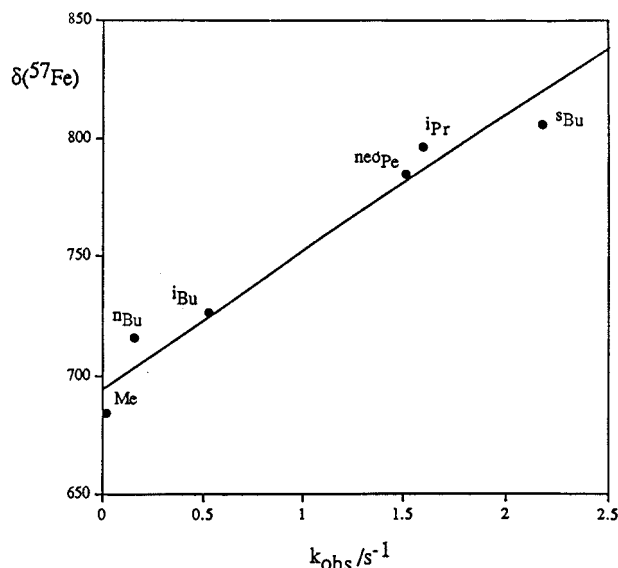
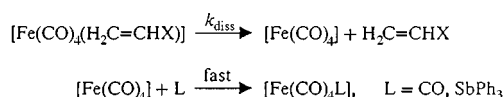


**Fig. 8** Correlation between the CO insertion rate,  $k_{\text{obs}}$ , for the reaction in Scheme 5 and  $\delta(^{57}\text{Fe})$  of the reactant complexes;  $R = 0.976$ , reproduced with permission from E. J. M. Meier, W. Kozminski, A. Linden, P. Lustenberger and W. von Philipsborn, *Organometallics*, 1996, **15**, 2469. Copyright (1996) American Chemical Society.

$< r^{-3} >$  term in eqn. (1). The longer Fe–C  $\sigma$ -bond will result in a larger  $< r^{-3} >$  term (nephelauxetic effect) leading to decreased  $^{57}\text{Fe}$  shielding. However, if the weaker Fe–C bond is associated with a smaller HOMO–LUMO gap, the  $\Delta E$  term may also be responsible for the deshielding effect.

The two examples of chemical shift–reactivity correlations for ligand exchange reactions in Schemes 4 and 5 are characterized by an *associative* mechanism, the attack of the nucleophile is facilitated by electron-attracting substituents, and a positive slope of the linear correlation is obtained (Figs. 6 and 8). The kinetics of the demetalation reaction of (olefin) $\text{Fe}(\text{CO})_4$  complexes with  $\text{SbPh}_3$  (or CO) were studied by Cardaci<sup>26</sup> and involve a rate-determining *dissociative* step followed by rapid reaction of the  $\text{Fe}(\text{CO})_4$  intermediate with  $\text{SbPh}_3$  (or CO) (Scheme 6). As expected for this dissociative mechanism,



**Scheme 6**

electron-donor substituents X increase the rate of the reaction and, thus, the rate *vs.*  $\delta(^{57}\text{Fe})$  correlation has a negative slope (Fig. 9). The same applies to the analogous reaction with CO as nucleophile.<sup>27</sup>

At this stage of the empirically established chemical shift *vs.* reactivity correlations, it appears that the reactivity-controlling influence of the substituents in the transition state of the respective reaction is also exerted with the same trend on the reactant complex, a behaviour that can be expected if an *early reactant-like* transition state is formed. Then the question arises whether such correlations can also be observed when a *late, product-like* transition state is involved and the chemical shift of the product complex is plotted against the reaction rate.

An example of this type is provided in Fig. 10 in which the substituent dependence of the  $\text{PPh}_3$  induced rate of aryl migration in  $\text{Cp}(\text{Me}_5)\text{Rh}(\text{I})(\text{Co})(\text{aryl})$  complexes is plotted as a function of the  $^{103}\text{Rh}$  chemical shift in the substituted benzoyl complexes **2**<sup>24</sup> (Scheme 7). The data in Table 4 clearly show that the  $^{103}\text{Rh}$  chemical shifts in the reactant complexes **1** vary little and do *not* give a significant correlation with the rate data ( $R^2 = 0.813$ ) whereas the product correlation is very high ( $R^2 =$

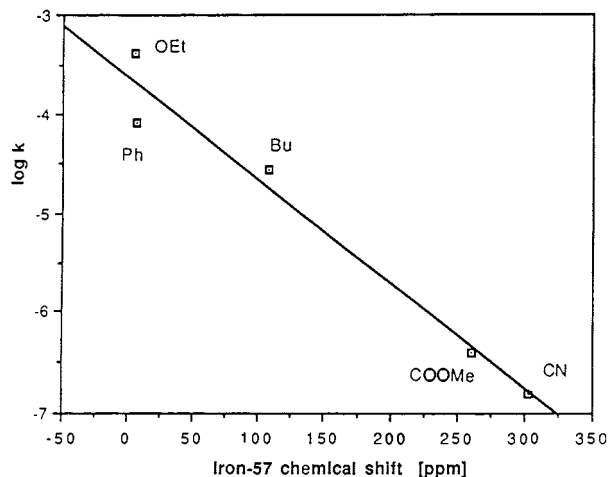


**Fig. 9** Plot of  $\log k_{\text{diss}}$  against  $\delta(^{57}\text{Fe})$  of the dissociative ligand exchange  $\text{CH}_2=\text{CHX} \rightarrow \text{SbPh}_3$  in  $[\text{Fe}(\text{CO})_4(\text{H}_2\text{C}=\text{CHX})]$  complexes (Scheme 6),  $R^2 = 0.96$ .<sup>27</sup>

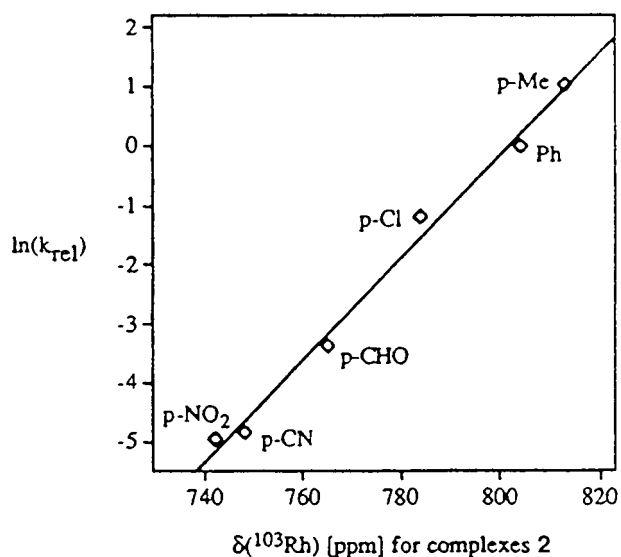
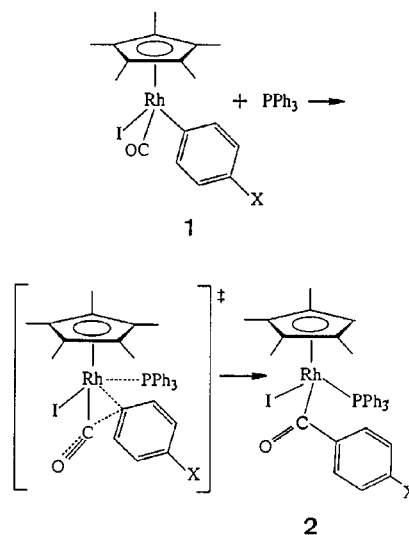


**Fig. 10** Correlation of relative rate constants  $k_{\text{rel}}$  *vs.*  $^{103}\text{Rh}$  chemical shifts of the *product* complexes **2** from the  $\text{PPh}_3$ -assisted aryl migration (Scheme 7),  $R^2 = 0.991$ ; reproduced with permission from V. Tedesco and W. von Philipsborn, *Organometallics*, 1995, **14**, 3600. Copyright (1995) American Chemical Society.



**Scheme 7**

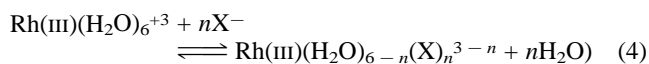
**Table 4**  $^{103}\text{Rh}$  Chemical shifts ( $\pm 1$  ppm,  $\text{CDCl}_3$ , 300 K) of complexes **1** and **2** in Scheme 7 and rel. rates for the reaction **1**  $\rightarrow$  **2**

R	$\delta(\text{Rh})$ <b>1</b>	$\delta(\text{Rh})$ <b>2</b>	$k_{\text{rel}}$
<i>p</i> -MeC <sub>6</sub> H <sub>4</sub>	-106	813	2.8
Ph	-102	804	1
<i>p</i> -ClC <sub>6</sub> H <sub>4</sub>	-122	784	0.31
<i>p</i> -OHCC <sub>6</sub> H <sub>4</sub>	-121	765	0.034
<i>p</i> -NCC <sub>6</sub> H <sub>4</sub>	-127	748	0.008
<i>p</i> -O <sub>2</sub> NC <sub>6</sub> H <sub>4</sub>	-134	742	0.007

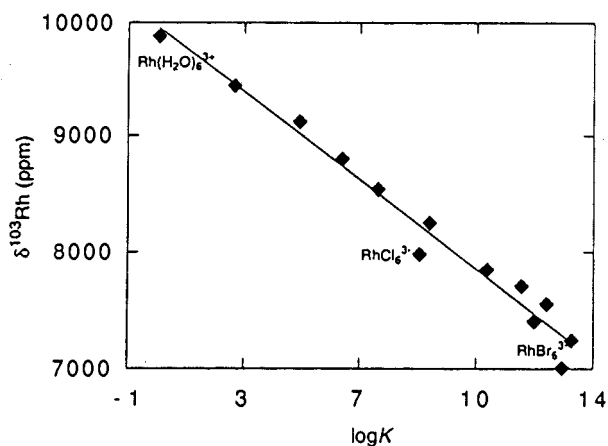
0.991). A plot of  $\sigma_p$  (Hammett electronic parameter) against  $\delta(\text{Rh})$  of the product complexes **2** is also linear with the correlation coefficient  $R^2 = 0.991$ .

This first example of a correlation between transition-metal chemical shifts of the reaction product with rate data enables us to postulate that the aryl migration proceeds *via* a late transition state which is structurally more similar to the product than the reactant. This implies that in the transition state the C(aryl)-C(O) and Rh-PPh<sub>3</sub> bonds are already formed to an appreciable extent with simultaneous breaking of the Rh-C(aryl) bond.

The importance of rhodium as a constituent of homogeneous catalysts has induced several research groups to investigate  $^{103}\text{Rh}$  NMR as a probe into complex stability and catalytic activity. Öhrström<sup>14</sup> has found that the rhodium chemical shift correlates linearly with the thermodynamic stability constants of the replacement of one ethylene unit in Rh(acac)(ethylene)<sub>2</sub> by propene, *cis*- and *trans*-butene and, in another case, with the overall stability constants for the formation of Rh(H<sub>2</sub>O)<sub>*n*</sub>X<sub>*m*</sub><sup>3-*m*</sup> complexes in water (Fig. 11, eqn. (4)).

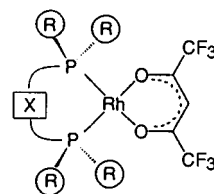


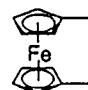
The theoretical rationale for this relationship was given based on ligand field theory and the  $\Delta E$  term of the paramagnetic shift eqn. (1). Further examples for this relationship of the type  $\delta = m - k \times \log K$  are supplied using  $^{59}\text{Co}$  and  $^{195}\text{Pt}$  shielding data.<sup>14</sup> In all cases, metal shielding decreases with decreasing complex stability.



**Fig. 11** The correlation of  $^{103}\text{Rh}$  chemical shifts with overall stability constants  $\log K$  for the formation of Rh(H<sub>2</sub>O)<sub>*n*</sub>(X)<sub>*m*</sub><sup>3-*m*</sup> complexes in H<sub>2</sub>O, according to eqn. (4); reproduced with permission from L. Öhrström, *Comments Inorg. Chem.*, 1996, **18**, 305. Copyright (1996) Overseas Publishers Association, Amsterdam B.V.

There is a logical step from the stability of transition metal complexes to catalytic activity which is dependent on the ease of ligand exchange. Leitner *et al.* have investigated complexes of the type [P<sub>2</sub>Rh(hfacac)] (P<sub>2</sub> = bidentate chelating phosphane, hfacac = hexafluoroacetylacetonate) as catalysts in the hydrogenation of CO<sub>2</sub> to formic acid<sup>28</sup> (Scheme 8). They found that the P-Rh-P valence angle, as determined from X-ray diffraction, correlates linearly with the  $^{103}\text{Rh}$  chemical shift in eight complexes ( $R = 0.970$ ) according to eqn. (5) (Fig. 12).



	X = (CH <sub>2</sub> ) <sub>2</sub>	R = Ph
<b>1a</b>	(CH <sub>2</sub> ) <sub>2</sub>	Ph
<b>1b</b>	(CH <sub>2</sub> ) <sub>2</sub>	Cy
<b>1c</b>	(CH <sub>2</sub> ) <sub>2</sub>	<i>i</i> Pr
<b>1d</b>	(CH <sub>2</sub> ) <sub>2</sub>	Me
<b>1e</b>	(CH <sub>2</sub> ) <sub>3</sub>	Ph
<b>1f</b>	(CH <sub>2</sub> ) <sub>4</sub>	Ph
<b>1g</b>	(CH <sub>2</sub> ) <sub>4</sub>	Cy
<b>1o</b>		<i>i</i> Pr

**Scheme 8**

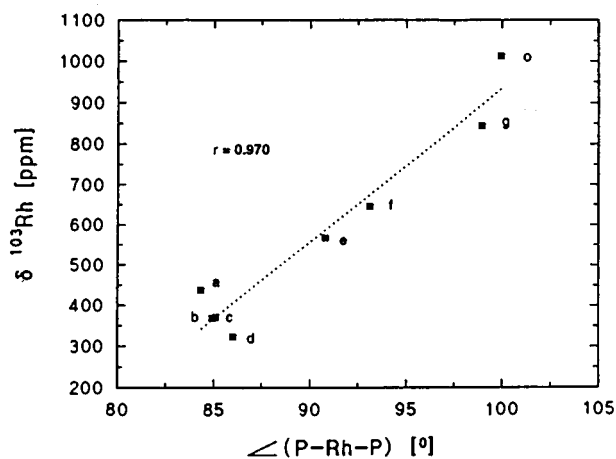
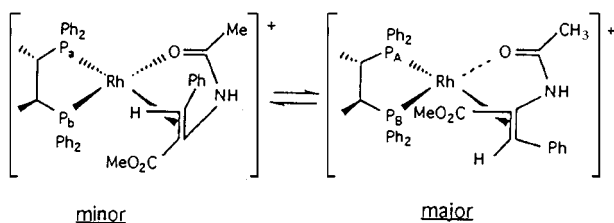


**Fig. 12**  $^{103}\text{Rh}$  Chemical shifts and P-Rh-P angles as obtained from X-ray crystal structures in [(P<sub>2</sub>)Rh(hfacac)] complexes (Scheme 8),  $R = 0.970$ ; reproduced with permission from K. Angermund, W. Baumann, E. Dinjus, R. Fornika, H. Görls, M. Kessler, C. Krüger, W. Leitner and F. Lutz, *Chem. Eur. J.*, 1997, **3**, 755. Copyright (1997) Wiley-VCH.

$$\delta(^{103}\text{Rh}) = -2361.5 + 32 \times (\text{PRhP angle}/^\circ) \quad (5)$$

The complexes with the largest P-Rh-P angle and, hence, the least shielded Rh nuclei, are the most effective catalysts, as measured by the rate (turnover frequency) of formic acid formation. In this case, the variation in the  $^{103}\text{Rh}$  chemical shifts is primarily due to steric effects in the coordination by the bidentate phosphane ligand.

One of the best studied examples in homogeneous catalysis is provided by the Rh-catalyzed hydrogenation of prochiral olefins. When chiral rhodium(diphosphane) complexes are used as catalysts, two diastereomeric substrate-catalyst complexes (Scheme 9) are formed that are in equilibrium and exhibit very different reactivity towards molecular hydrogen. Halpern was able to show by careful kinetic studies<sup>29</sup> that the major isomer is rather unreactive and the catalysis is effected *via* the highly reactive minor isomer present in usually less than 10% rel. concentration. For a long time, the large difference in reactivity of the two diastereomeric intermediates has remained a mystery as the minor isomers were not very well characterized by physical methods. The general opinion prevailed that different



Scheme 9

stereochemical situations are the dominant factors. However, the picture changed with the results from a detailed  $^{103}\text{Rh}$  NMR study of the system for a variety of substituted enamine substrates and achiral (diphos) and chiral (chiraphos and dipamp) phosphane complexes.<sup>30</sup> Firstly, the large shielding difference between the Rh nuclei in the major and minor diastereoisomers ( $\Delta\delta = 30\text{--}250$  ppm) was surprising, whereby the reactive minor isomer is always *deshielded* relative to the major one (Fig. 13). Secondly, large chemical shift effects arise

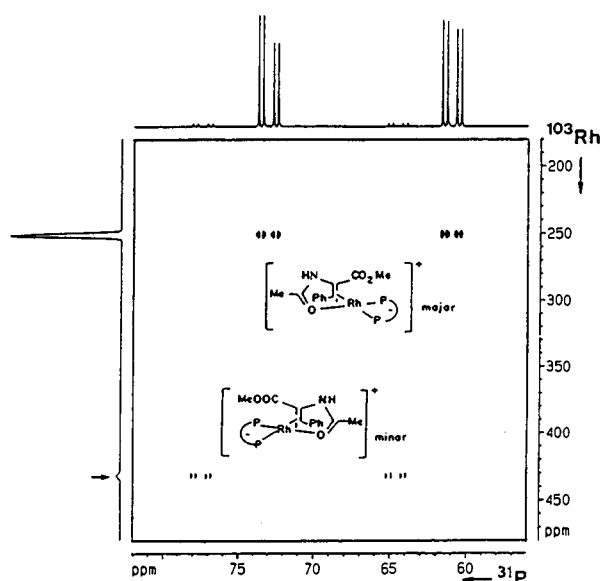


Fig. 13 2D ( $^{31}\text{P}$ ,  $^{103}\text{Rh}$ )- $\{^1\text{H}\}$  shift-correlation spectrum for [(methyl *Z*- $\alpha$ -N-acetamidocinnamate)Rh(SS-chiraphos)] $[\text{ClO}_4]$  showing the  $^{103}\text{Rh}$  resonances of the major and minor diastereoisomers on the  $F_1$  axis; reproduced with permission from B. R. Bender, M. Koller, D. Nanz and W. von Philipsborn, *J. Am. Chem. Soc.*, 1993, **115**, 5889. Copyright (1993) American Chemical Society.

from electronic substituent effects, whereas the effect of steric perturbation is small. Thus it was concluded that the enantioselectivity of the hydrogenation of enaminoesters to optically active  $\alpha$ -amino acids is caused by electronic differences *at rhodium* and the olefinic ligand is more tightly coordinated to the metal in the major diastereomer augmenting the key two-orbital, four electron repulsion in the hydrogen attack. It should be noted that the lower shielding of the Rh nucleus in the reactive minor diastereomer matches the relative stability *vs.* chemical shift correlations by Öhrström.<sup>14</sup> In other words, increased shielding of the transition metal appears to indicate stronger bonding of the substrate which, in turn, renders the metal less reactive toward adding another ligand. The detection and characterization of the minor diastereomer by Rh NMR is an excellent example of the high sensitivity of state-of-the-art NMR techniques which considerably extend the spectroscopic arsenal of the structural and mechanistic organometallic chemist.

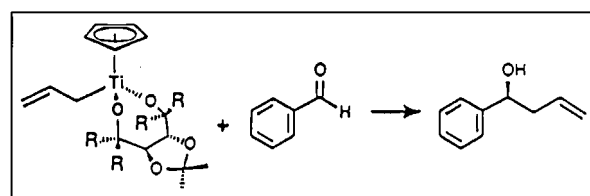
Öhrström<sup>14</sup> has discussed the question to what extent the observed difference  $\Delta\delta(\text{Rh})$  for the two diastereomeric complexes could be related to their different reactivities in more than a qualitative sense. It was suggested that for this purpose

the components of the chemical shift tensor might be more relevant than the trace of the tensor measured in the isotropic chemical shift. However, the increasing number of successful correlations of chemical shifts with reaction rates cannot be fortuitous. Most recently, an example was reported in which the chemical shifts of the non-metallic nucleus  $^{17}\text{O}$  were correlated with the rates of a manganese demetalation reaction.<sup>1</sup>

Another early attempt to correlate reactivity with transition metal NMR data was made by Hafner *et al.* in the series of pentacarbonylchromium(carbene) complexes.<sup>31</sup> Whereas no correlation with the  $^{53}\text{Cr}$  chemical shifts could be observed in a wide range of 46 different carbene complexes, it appeared as if the line width  $\Delta\nu(1/2)$  of the chromium resonance was larger for the reactive complexes, while complexes with narrow lines failed to react in photolytic reactions with imines to yield  $\beta$ -lactams. Unfortunately, this study did not allow for the additional influence on  $\Delta\nu(1/2)$  of varying correlation times  $\tau_c$  along with electronic structural factors that could be reflected in the reactivity, eqn. (6).

$$\Delta\nu(1/2) \propto q_{zz}^2 \cdot \left(1 + \frac{\eta^2}{3}\right) \cdot \tau_c \quad (6)$$

A second example was discussed by Hafner *et al.*<sup>32</sup> in which the enantioselectivity of allyltitanation of aldehydes with cyclopentadienyl-dialkoxyallyltitanium complexes (Scheme 10) appears to be related to electronic dissymmetry at titanium



R	$\Delta\nu_{1/2}(^{49}\text{Ti})$	% ee
CH <sub>3</sub>	1080 [Hz]	13
C(CH <sub>3</sub> )=CH <sub>2</sub>	1400	71
C <sub>6</sub> H <sub>5</sub>	3460	95

Scheme 10 Reproduced with permission from A. Hafner, R. O. Duthaler, R. Marti, G. Rihs, P. Rothe-Streit and F. Schwarzenbach, *J. Am. Chem. Soc.*, 1992, **114**, 2321. Copyright (1992) American Chemical Society.

reflected in the relative line widths of the  $^{49}\text{Ti}$  NMR resonances of the reagents. However, the significance of this observation in three cases needs to be confirmed on a broader data basis, including also measurements of rotational correlation times  $\tau_c$ . In fact, the expected change in the correlation times  $\tau_c$  of the respective compounds parallels the trend in the observed line widths  $\Delta\nu(1/2)$  of the  $^{49}\text{Ti}$  resonances.

The quadrupolar relaxation rate  $T_2^{-1}$  is indeed strongly dependent on the electric field gradient  $q_{zz}$  and, hence, on the coordination geometry at the metal. This was recently shown by us in a detailed study of the  $^{91}\text{Zr}$  resonance in zirconocene complexes, the second generation of Ziegler-Natta catalysts for the stereoregular polymerization of olefins.<sup>33</sup> As a major result of this experimental NMR investigation, supported by quantum chemical calculations, it can be concluded that the  $^{91}\text{Zr}$  NMR line width of zirconocenes is dominated, for the *smaller* substituted complexes, by the variations in the electric field gradient  $q_{zz}$  and for the *larger* complexes by changes in the isotropic molecular correlation time  $\tau_c$  [eqn. (6)].

Since only the field gradient is directly related to electronic and steric ligand effects, the experimental line width does not



appear to be a suitable probe into complex reactivity unless  $\tau_c$  does not vary significantly.

Many homogeneous catalysts contain phosphorus ligands that can be used to fine-tune catalyst activity and selectivity. The transition metal chemical shift has proven a very sensitive probe to mirror such ligand effects. In particular, the  $^{57}\text{Fe}$  and  $^{187}\text{Os}$  chemical shifts were shown to give excellent linear correlations with the Tolman cone angle  $\theta$  of the substituted phosphane.<sup>5,34</sup> An example is illustrated in Fig. 14 for (*p*-

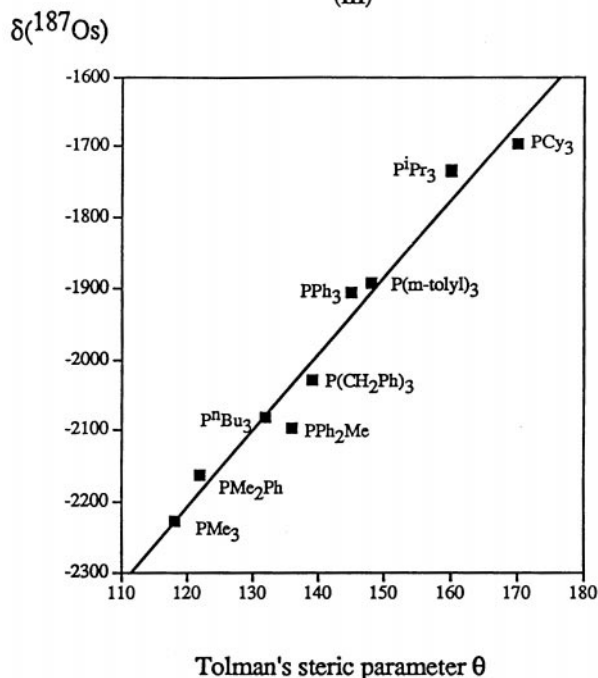
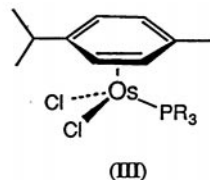


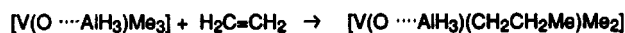
**Fig. 14** Plot of  $\delta(^{187}\text{Os})$  vs. Tolman's steric parameter  $\theta$  (cone angle) for (*p*-cymene) $\text{Os}(\text{Cl})_2\text{PR}_3$  complexes,  $R^2 = 0.97$ ; reproduced with permission from A. G. Bell, W. Kozminski, A. Linden and W. von Philipsborn, *Organometallics*, 1996, **15**, 3124. Copyright (1996) American Chemical Society.

cymene) $\text{Os}(\text{Cl})_2\text{PR}_3$  complexes which serve as models for the analogous ruthenium complexes that are highly active in olefin polymerization. Shielding of the  $^{187}\text{Os}$  nucleus decreases with increasing  $\theta$  or increasing catalytic activity. Also this correlation may be used in an efficient screening of complexes for catalytic activity. It has furthermore been applied to revise the Tolman angles that were reported for  $\text{P}(\text{CH}_2\text{Ph})_3$  and  $\text{P}(m\text{-tolyl})_3$ .<sup>34</sup> The high sensitivity of osmium shielding is also exemplified by the substituent effects of alkyl groups attached to the benzene ring in complexes of the type  $(\text{C}_6\text{H}_5\text{R})\text{Os}(\text{Cl})_2\text{PMe}_3$  with chemical shifts ranging from  $-2431$  ppm for  $\text{R} = \text{H}$  to  $-2268$  ppm for  $\text{R} = ^t\text{Bu}$  and providing an excellent linear correlation ( $R = 0.99$ ) with Taft's steric substituent parameter  $E_s$ .

## 5 Quantum chemical *ab-initio* calculations

Very recently, the empirical correlations between the chemical shifts of various transition metals and reactivity data have stimulated theoretical chemists to perform *ab-initio* quantum chemical calculations to establish a theoretical basis for these observations. Density-functional theory (DFT) has proved

particularly suitable for a calculation of reactivities and chemical shifts.<sup>35,36</sup> A pertinent example is the calculation of the  $^{51}\text{V}$  chemical shifts for  $[\text{VOCl}_n\text{F}_{3-n}]$  ( $n = 0-3$ ),  $\text{VF}_5$ ,  $[\text{VO}(\text{OCH}_2\text{CH}_2)_3\text{N}]$ ,  $[\text{V}(\text{CO})_6]^-$ ,  $[\text{V}(\text{CO})_5(\text{N}_2)]^-$ , as well as for the model compounds  $[\text{VO}(\text{OMe})_n\text{Me}_{3-n}]$  ( $n = 0-3$ ) and their  $\text{AlH}_3$  adducts. A very satisfactory agreement between calculated and experimental shielding data has been attained. Silica-supported vanadium catalysts have found considerable interest in olefin polymerization but the detailed mechanism is still being discussed. The theoretical study has advanced a plausible mechanism by which ethylene is inserted into the  $\text{V}-\text{C}$  bond of the  $[\text{V}(\text{O}\cdots\text{AlH}_3)\text{Me}_3]$  complex in a rate-determining step (Scheme 11). The DFT-derived activation barriers  $\Delta E_a$  and



Scheme 11

calculated  $^{51}\text{V}$  chemical shifts for different Lewis acid adducts are correlated as shown in Fig. 15. Also in this case it is

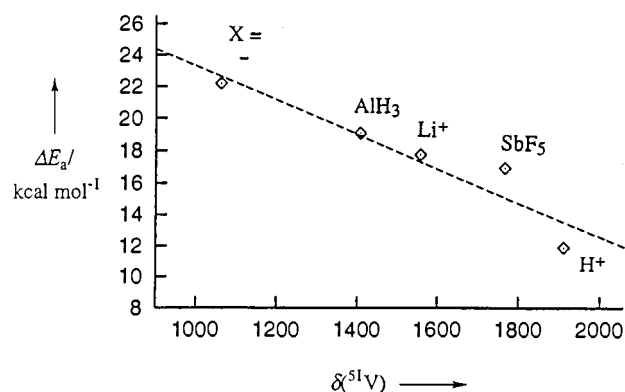


**Fig. 15** Correlation of DFT-derived barriers to ethene insertion  $\Delta E_a$  and calculated  $^{51}\text{V}$  chemical shifts for the Lewis acid adducts  $[\text{V}(\text{O}\cdots\text{X})\text{Me}_3]$ ; reproduced with permission from M. Bühl, *Angew. Chem., Int. Ed. Engl.*, 1998, **37**, 142. Copyright (1998) Wiley-VCH.

observed that the least shielded metal resonance is associated with the lowest activation energy, *i.e.* the (probably) most reactive catalyst. This result constitutes the first theoretical prediction of such an NMR–reactivity correlation and calls for experimental verification. However, it was clearly stated by the authors<sup>35</sup> that there appears to be no intrinsic relationship between these properties, and thus further calculations are required to bring such correlations beyond the empirical stage.

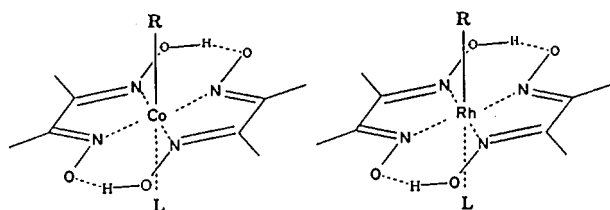
Similar *ab-initio* calculations using the SOS-DFPT approach have lent theoretical support to the  $^{103}\text{Rh}$  chemical shift–reactivity correlation observed for  $\text{CO}-\text{PPh}_3$  ligand exchange in  $[(\text{C}_5\text{H}_4\text{X})\text{Rh}(\text{CO})_2]$  complexes (Fig. 6). In the  $\text{PH}_3$  model system the calculated activation energies for  $\text{X} = \text{NMe}_2$ ,  $\text{Cl}$ , and  $\text{NO}_2$  show the same trend as the experimental rate constants.<sup>36</sup> Also the computed  $^{103}\text{Rh}$  chemical shifts agree with the experimental data within less than 100 ppm deviation. Furthermore, these calculations have shown that the reaction proceeds *via* a ‘ring slipped’  $\eta^3$ -intermediate with an uncoordinated double bond in the cyclopentadienyl ring.

With the same theoretical approach applied to the  $\text{CpFe}(\text{CO})_2\text{R}$  system and the  $\text{PPh}_3$ -induced  $\text{CO}$  insertion into the  $\text{Fe}-\text{C}$  bond (Scheme 5 and Fig. 8) consistency of the computed  $\text{Fe}-\text{C}(\text{alkyl})$  bond dissociation energies and the trend in the experimental rate constants was demonstrated. Both direction and magnitude of the substituent  $\text{R}$  dependence of  $\delta(^{57}\text{Fe})$  are well described.<sup>36,5</sup>

In the near future such calculations will constitute an important contribution to a deeper understanding of mechanistic organometallic chemistry in general and, more specifically, of transition metal NMR shielding in organometallic and coordination compounds.

## 6 Miscellaneous studies

This progress report has mainly dealt with the present state of knowledge regarding correlations between transition metal shielding and organometallic reactivity. In this respect, the metal–carbon  $\sigma$ -bond deserves particular attention as it is involved in numerous important transformations, such as metathesis of olefins and various insertion-type reactions, but even enzymatic reactions related to coenzyme-B<sub>12</sub> and methylcobalamine make use of this reactive bond system. Several attempts have been made to rationalize the special reactivity of the Co–C bond in the coenzyme and model cobaloxime complexes (Scheme 12).



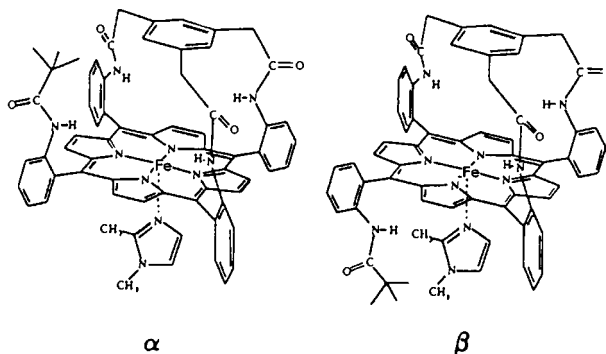
Scheme 12

Using <sup>59</sup>Co NMR it was found<sup>13,16</sup> that shielding decreases with increasing bulk of the alkyl group attached to the cobalt centre and that the Co–C bond lengths show a parallel increase. The chemical shifts  $\delta(^{59}\text{Co})$  correlate with Taft's steric parameter  $E_s$ , but not with Hammett's electronic  $\sigma^*$  parameter. These findings indicate a weakening of the organometallic bond with increasing size or branching of the alkyl group in agreement with the results on alkyliron complexes discussed in Section 4. The generality of the phenomenon of steric deshielding of transition metal nuclei is supported by the facts that in alkylrhodoximes (Scheme 12) the same effect was observed,<sup>17</sup> and that  $\delta(^{59}\text{Co})$  correlates linearly with  $\delta(^{103}\text{Rh})$  for R = Me, Et, <sup>i</sup>Pr, <sup>n</sup>Bu and <sup>neo</sup>Pent with a slope of 2.1. The greater sensitivity of cobalt agrees with the rel. ionic radii of Co(III) (64 pm) and Rh(III) (75 pm) and supports the steric nature of the effect.

The presence of the spin-1/2 nucleus <sup>103</sup>Rh in the rhodoximes has the added advantage of greater precision in the chemical shift determination and gives access to spin coupling parameters, such as  $J(^{103}\text{Rh},^{13}\text{C})$ ,  $J(^{103}\text{Rh},^{31}\text{P})$ , and  $J(^{103}\text{Rh},^{15}\text{N})$ . It turned out, however, that  $^1J(\text{Rh},\text{C})$  does not vary a great deal in the series of alkylrhodoximes ( $J = 23\text{--}26$  Hz) and can hardly be useful as a probe into the metal–carbon bond, in contrast with the large chemical shift range of about 180 ppm for eight complexes with alkyl substituents ranging from methyl to adamantyl.

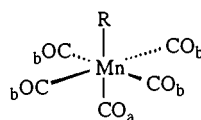
Transition metal NMR studies have been conducted in large biological molecules as well as, e.g., of the cobalt centre in vitamin-B<sub>12</sub> and methylcobalamine<sup>3</sup> and, more recently, of the iron centre in heme proteins and superstructured (bridged) hemoprotein model complexes.<sup>38</sup> Whereas the <sup>59</sup>Co NMR measurement can be conducted at natural (100%) isotope abundance, the very low receptivity of the <sup>57</sup>Fe nucleus (Table 1) requires high isotopic enrichment (95%). However, it was possible to demonstrate that the carbon monoxide complexes of the two  $\alpha$ - and  $\beta$ -atropisomers (Scheme 13) give rise to widely separated <sup>57</sup>Fe resonance lines ( $\Delta\delta = 158$  ppm) which is attributed to a different degree of ruffling of the porphyrin ligand and iron-d-orbital perturbation. In contrast, the <sup>57</sup>Fe,<sup>13</sup>CO one-bond coupling constants are almost the same (25–26 Hz) for the two isomers and do not reflect the large electronic differences at the iron atom which parallels the observations in alkylrhodoximes.<sup>17</sup>

Metal–carbon spin coupling constants become more useful as a structural probe when the metal nucleus has a magnetic moment larger than <sup>57</sup>Fe and <sup>103</sup>Rh. As an example, <sup>55</sup>Mn,<sup>13</sup>C

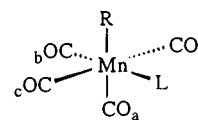


Scheme 13 Reproduced with permission from I. P. Gerotheranassis, C. G. Kalodimos, G. Hawkes and P. Haycock, *J. Magn. Reson.*, 1998, **131**, 163. Copyright (1998) Academic Press.

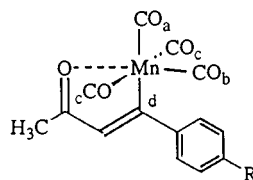
coupling constants can serve as an indicator of the metal–carbon bond order. Although the quadrupolar <sup>55</sup>Mn nucleus has short relaxation times and causes broad, unresolved <sup>13</sup>C resonance lines it has been shown that the spin coupling constants can be extracted by careful line-shape analysis.<sup>39</sup> The results were checked against corresponding data from solid-state MAS-NMR spectra, and very good agreement was achieved. As illustrated in Scheme 14,  $^1J(\text{Mn},\text{C})$  coupling constants vary



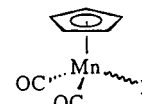
I R = alkyl, acyl, halide  
hydride



II R = alkyl, acyl, halide  
L = phosphane, amine,  
isocyanide



III R = OMe, Me, H, Cl, NO<sub>2</sub>



IVa R = carbene  
IVb R = carbene

complex	bond	$^1J(\text{Mn},\text{C})$ [Hz]
I, II	Mn–C(R)	35–64
III	Mn–C=C	65–81
IVa	Mn=C	97–131
IVb	Mn≡C	168–188

Scheme 14 Reproduced with permission from D. Rentsch, PhD Thesis, University of Zürich, 1997.

between 35 and 190 Hz and increase with the Mn–C bond order. Mn,CO coupling constants may become even larger (130–220 Hz) and substituent effects on  $J(\text{Mn},\text{CO})$  are particularly noticeable when the carbonyl group is in a diaxial arrangement with the substituent R, thus illustrating a typical 'trans-effect', as in the case of (CO)<sub>a</sub>.

Because of the still limited data base on metal–carbon coupling constants this parameter has not yet been explored to

the same extent as the metal chemical shifts in probing structure and bond reactivity in organometallic chemistry, but more applications of this kind can be expected.

## 7 Concluding remarks

Significant improvements in the NMR detection of transition metal nuclei, both spin-1/2 and quadrupolar, have opened this much neglected field of NMR spectroscopy for a wide range of applications in organometallic and coordination chemistry. Besides a detailed insight into the coordination sphere of the metal, stereochemistry, and metal–ligand bonding, the most promising and truly novel application lies in the apparent relation between metal shielding and reactivity. A number of quantitative correlations involving  $^{51}\text{V}$ ,  $^{55}\text{Mn}$ ,  $^{57}\text{Fe}$ ,  $^{59}\text{Co}$ ,  $^{103}\text{Rh}$ , and  $^{187}\text{Os}$  nuclei with the rate constants of ligand exchange reactions, both associative and dissociative, have revealed that within families of structurally closely related compounds substituent effects on reaction rates and transition metal shielding (chemical shifts) of reactant (or product) show largely parallel trends. The sign of the slope of the observed linear correlations depends upon the mechanism of the reaction, e.g. it differs for associative and dissociative ligand displacements as well as for reactions driven by acceptor or donor ligands, respectively. A new concept has been proposed that connects reactant-related correlations with reactant-like (early) transition states, while product-related correlations point towards product-like (late) transition states for the rate-determining steps. The shielding–reactivity correlations can be extended to catalytic systems and may be used in reactivity screening of potential homogeneous catalysts by a determination of their metal chemical shift.

In some cases, the empirical correlations and trends were confirmed by quantum chemical calculations using *ab-initio* and DFT methods applied to ground state and transition state electronic configurations. It appears, however, that there is no *intrinsic* relationship between nuclear shielding and reactivity in transition metal complexes, and thus further detailed calculations of empirically established ‘successful cases’ are required in order to achieve a deeper understanding of the experimental observations. There can be little doubt, however, that the already established examples of chemical shift–reactivity correlations will have an impact on structural and synthesis-oriented organometallic chemists, and further applications in homogeneous catalysis can be envisaged as well.

## 8 Acknowledgements

The author would like to express his indebtedness to numerous graduate students and postdoctoral coworkers who have been involved in the experimental work from our laboratory and are mentioned in the respective references.

Furthermore, stimulating discussions with my colleagues P. DeShong (Maryland), H.-H. Brintzinger and H. Fischer (Konstanz), G. Costa and G. Pellizer (Trieste), and M. Bühl (Zürich) are gratefully acknowledged.

Our work has found generous support from the Swiss National Science Foundation, the Dr Helmut Legerlotz-Stiftung, the Kanton Zürich, and Bruker-Spectrospin.

## 9 References

- 1 D. Rentsch, L. Nill, W. von Philipsborn, D. R. Sidler, P. J. Rybczynski and P. DeShong, *Magn. Reson. Chem.*, 1998, **36**, S54.
- 2 *Transition Metal Nuclear Magnetic Resonance*, ed. P. S. Pregosin, 1991, Elsevier, Amsterdam.
- 3 W. von Philipsborn, *Pure Appl. Chem.*, 1986, **58**, 513.
- 4 R. Benn and A. Rufinska, *Angew. Chem., Int. Ed. Engl.*, 1986, **25**, 861.
- 5 E. J. M. Meier, W. Kozminski, A. Linden, P. Lustenberger and W. von Philipsborn, *Organometallics*, 1996, **15**, 2469, and refs. cited therein.
- 6 D. Rehder, *Coord. Chem. Rev.*, 1991, **110**, 161.
- 7 *Multinuclear NMR*, ed. J. Mason, 1987, Plenum Press, New York.
- 8 L. Müller, *J. Am. Chem. Soc.*, 1979, **101**, 4481.
- 9 A. Bax, R. H. Griffey and B. L. Hawkins, *J. Am. Chem. Soc.*, 1983, **105**, 7188.
- 10 R. Benn and C. Brevard, *J. Am. Chem. Soc.*, 1986, **108**, 5622.
- 11 D. Nanz, *Indirekte Detektion in der NMR-Spektroskopie metallorganischer Systeme, Konzepte und Anwendungen*, PhD Thesis, University of Zürich, 1993.
- 12 *NMR and the Periodic Table*, eds. R. K. Harris and B. E. Mann, 1978, Academic Press, London, ch. 3.
- 13 C. Tavagnacco, G. Balducci, G. Costa, K. Täschler and W. von Philipsborn, *Helv. Chim. Acta*, 1990, **73**, 1469.
- 14 L. Öhrström, *Comments Inorg. Chem.*, 1996, **18**, 305.
- 15 E. Maurer, S. Rieker, M. Schollbach, A. Schwenk, T. Egolf and W. von Philipsborn, *Helv. Chim. Acta*, 1982, **65**, 26.
- 16 K. Täschler, *Beiträge zur  $^{59}\text{Co}$ -Kernresonanz metallorganischer Verbindungen*, PhD Thesis, University of Zürich, 1990.
- 17 F. Asaro, G. Costa, R. Dreos, G. Pellizer and W. von Philipsborn, *J. Organomet. Chem.*, 1996, **513**, 193.
- 18 P. S. Pregosin and G. Trabesinger, *J. Chem. Soc., Dalton Trans.*, 1998, 727.
- 19 H. Bönemann, W. Brijoux, R. Brinkmann, W. Meurers, R. Mynott, W. von Philipsborn and T. Egolf, *J. Organomet. Chem.*, 1984, **272**, 231.
- 20 H. Bönemann, *Angew. Chem., Int. Ed. Engl.*, 1985, **24**, 248.
- 21 C. Marzin, F. Budde, P. J. Steel and D. Lerner, *Nouv. J. Chim.*, 1987, **11**, 33.
- 22 P. DeShong, D. R. Sidler, P. J. Rybczynski, A. A. Ogilvie and W. von Philipsborn, *J. Org. Chem.*, 1989, **54**, 5432.
- 23 M. Koller and W. von Philipsborn, *Organometallics*, 1992, **11**, 467.
- 24 V. Tedesco and W. von Philipsborn, *Organometallics*, 1995, **14**, 3600.
- 25 M. Cheong and F. Basolo, *Organometallics*, 1988, **7**, 2041.
- 26 G. Cardaci, *Int. J. Chem. Kinet.*, 1973, **5**, 805.
- 27 M. Koller, *CO-Austauschreaktionen an Metallcarbonyl(Olefin)-Komplexen*, PhD Thesis, University of Zürich, 1993.
- 28 K. Angermund, W. Baumann, E. Dinjus, R. Fornika, H. Görls, M. Kessler, C. Krüger, W. Leitner and F. Lutz, *Chem. Eur. J.*, 1997, **3**, 755.
- 29 C. R. Landis and J. Halpern, *J. Am. Chem. Soc.*, 1987, **109**, 1746, and refs. cited therein.
- 30 B. R. Bender, M. Koller, D. Nanz and W. von Philipsborn, *J. Am. Chem. Soc.*, 1993, **115**, 5889.
- 31 A. Hafner, L. S. Hegedus, G. de Weck, B. Hawkins and K. H. Dötz, *J. Am. Chem. Soc.*, 1988, **110**, 8413.
- 32 A. Hafner, R. O. Duthaler, R. Marti, G. Rihs, P. Rothe-Streit and F. Schwarzenbach, *J. Am. Chem. Soc.*, 1992, **114**, 2321.
- 33 M. Bühl, G. Hopp, W. von Philipsborn, S. Beck, M.-H. Prosenc, U. Rief and H.-H. Brintzinger, *Organometallics*, 1996, **15**, 778.
- 34 A. G. Bell, W. Kozminski, A. Linden and W. von Philipsborn, *Organometallics*, 1996, **15**, 3124.
- 35 M. Bühl and F. A. Hamprecht, *J. Comput. Chem.*, 1998, **19**, 113, and refs. cited therein.
- 36 M. Bühl, Habilitationsschrift, University of Zürich, 1997, and refs. cited therein.
- 37 M. Bühl, *Angew. Chem., Int. Ed. Engl.*, 1998, **37**, 142.
- 38 I. P. Gerathanassis, C. G. Kalodimos, G. Hawkes and P. Haycock, *J. Magn. Reson.*, 1998, **131**, 163, and refs. cited therein.
- 39 D. Rentsch, R. Hany and W. von Philipsborn, *Magn. Reson. Chem.*, 1997, **35**, 832, and refs. cited therein.

Review 7/06424A